Recent Results from H1

Josef Žáček

Institute of Particle and Nuclear Physics, Faculty of Mathematics and Physics
Charles University in Prague
V Holešovičkách 2, Praha 8, Czech Republic

Abstract

Selected H1 results obtained recently by studying various processes in ep collisions at a center-of-mass energy approximately 320 GeV at HERA are presented. The large event statistics has enabled to determine proton structure functions up to $Q^2 \sim 10^4$ GeV^2. The precise hadron reconstruction afforded to perform the detailed investigation of heavy flavor production. The jet measurements have been used to test QCD predictions and to study the QCD evolution of parton cascades. The proton diffractive parton densities have been extracted in the full available kinematic range. An excess of events above theoretical predictions has been observed in the final states with an isolated high transverse momentum lepton and missing transverse momentum and in multi-electron events. This effect has been confirmed in the general search for deviations of data from the Standard Model.

1 Introduction

During the first phase of HERA running between the years 1992-2000 positrons or electrons of the energy 27.5 GeV collided head on with protons of the energy of 820 GeV, which was increased to 920 GeV in the year 1998. The corresponding center-of-mass energies $\sqrt{s}$ are 301 and 318 GeV. The H1 experiment collected total integrated luminosity of ~ 115 pb^{-1}, out of which about 15 pb^{-1} were taken with the electron beam.

At fixed $\sqrt{s}$ the kinematics of the $e^{\pm}p$ interactions is described by two independent variables, the negative four momentum transfer squared Q^2 carried by the exchanged gauge boson (γ, Z_0, $W^{\pm}$) and either one of the scaling variables y, the inelasticity of the $e^{\pm}p$ scattering or by x-Bjorken. These variables are related via $Q^2 = sxy$. Due the large center-of-mass energy HERA experiments extended kinematic range by more than two orders magnitude in both, x and Q^2 with respect to that accessible by earlier fixed target experiments.

Lepton-proton interactions are detected in the H1 apparatus in various subdetectors surrounding the interaction region. A detailed description of the H1 detector can be found elsewhere [1], [2]. Here, the main components are introduced only. The central silicon tracker [3] and the backward silicon tracker [4] are mounted around the beam pipe. The interaction vertex is determined with the central tracking detector consisting of two large cylindrical jet drift chambers and two z drift chambers. The energy of scattered electrons[1] is measured in the liquid argon calorimeter (LAr), which covers a range in polar angle[2] between 4^o and 154^o. The electrons scattered with polar angles from 153^o to

[1] In the following, both electron and positron will be referred as electron.

[2] The polar angle of tracks θ is measured with respect to the z axis given by the proton beam direction.

177.5^o are detected in a calorimeter made of lead and scintillating fibers (SpaCal) [5]. The hadronic final states are reconstructed using the LAr calorimeter, SpaCal and the tracking chambers. The calorimeters are surrounded by an iron return yoke of the superconducting solenoid providing the uniform magnetic field of 1.15 T. Muons which penetrate the main detector are detected in the limited streamer tubes placed within the iron.

This report presents some of the most recent results obtained by analyzing data recorded between the years 1994 and 2000. Proton structure functions and parton distributions are discussed in section 2. Section 3 is devoted to the investigation of heavy quark production, followed by the presentation of results of the analysis of hadronic final states (section 4). Some selected topics of diffractive processes are mentioned in section 5. Finally, section 6 is dedicated to the search for new phenomena.

2 Inclusive Deep-Inelastic Scattering

The neutral current (NC) deep-inelastic (DIS) cross section for reaction $e^{\pm}p \to e^{\pm}X$ can be expressed in terms of three generalized structure functions $\tilde{F}_2$, $x\tilde{F}_3$ and $\tilde{F}_L$:

$$\frac{d^2\sigma^{\pm}_{NC}}{dxdQ^2} = \frac{2\pi\alpha^2}{xQ^4}[Y_+\tilde{F}_2 \mp Y_- \cdot x\tilde{F}_3 - y^2\tilde{F}_L] \tag{1}$$

where $Y_{\pm} = 1 \pm (1-y)^2$. The structure functions $\tilde{F}_2$ and $\tilde{F}_3$ can be further decomposed as [6]

$$\tilde{F}_2 \equiv F_2 + c_2^{\gamma Z}(Q^2) \cdot F_2^{\gamma Z} + c_2^Z(Q^2) \cdot F_2^Z \qquad x\tilde{F}_3 \equiv c_3^{\gamma Z}(Q^2) \cdot xF_3^{\gamma z} + c_3^Z(Q^2) \cdot xF_3^Z \tag{2}$$

where coefficients c_2 and c_3 are functions of known electroweak parameters. At HERA the dominant contribution to the cross section is due to F_2 which originates from photon exchange. Within the quark parton model the $\tilde{F}_2$ structure function is related to the sum of quark and anti-quark momentum distributions, $xq(x,Q^2)$ and $x\bar{q}(x,Q^2)$, whereas $x\tilde{F}_3$ to their difference.

The charge current (CC) reactions $e^-p \to \nu X$ ($e^+p \to \bar{\nu}X$) are mediated by the exchange of a W^- (W^+). The corresponding cross section can be written as

$$\frac{d^2\sigma^{\pm}_{CC}}{dxdQ^2} = \frac{G_F^2}{2\pi x}\left[\frac{M_W^2}{Q^2+M_W^2}\right]^2 \tilde{\sigma}^{\pm}_{CC} \tag{3}$$

where the reduced cross section $\tilde{\sigma}^{\pm}_{CC}$ is the combination of quark distributions (u, c, d, s) and anti-quark distributions ($\bar{u}$, $\bar{c}$, $\bar{d}$, $\bar{s}$)

$$\tilde{\sigma}^{+}_{CC} = x[\bar{u}(x,Q^2) + \bar{c}(x,Q^2) + (1-y)^2(d(x,Q^2) + s(x,Q^2))] \tag{4}$$

$$\tilde{\sigma}^{-}_{CC} = x[u(x,Q^2) + c(x,Q^2) + (1-y)^2(\bar{d}(x,Q^2) + \bar{s}(x,Q^2))] \tag{5}$$

The neutral and charged current cross sections have been measured by H1 experiment [6] up to the highest Q^2 of $\sim 10^4$ GeV^2. From these measurements structure functions and parton densities have been determined.

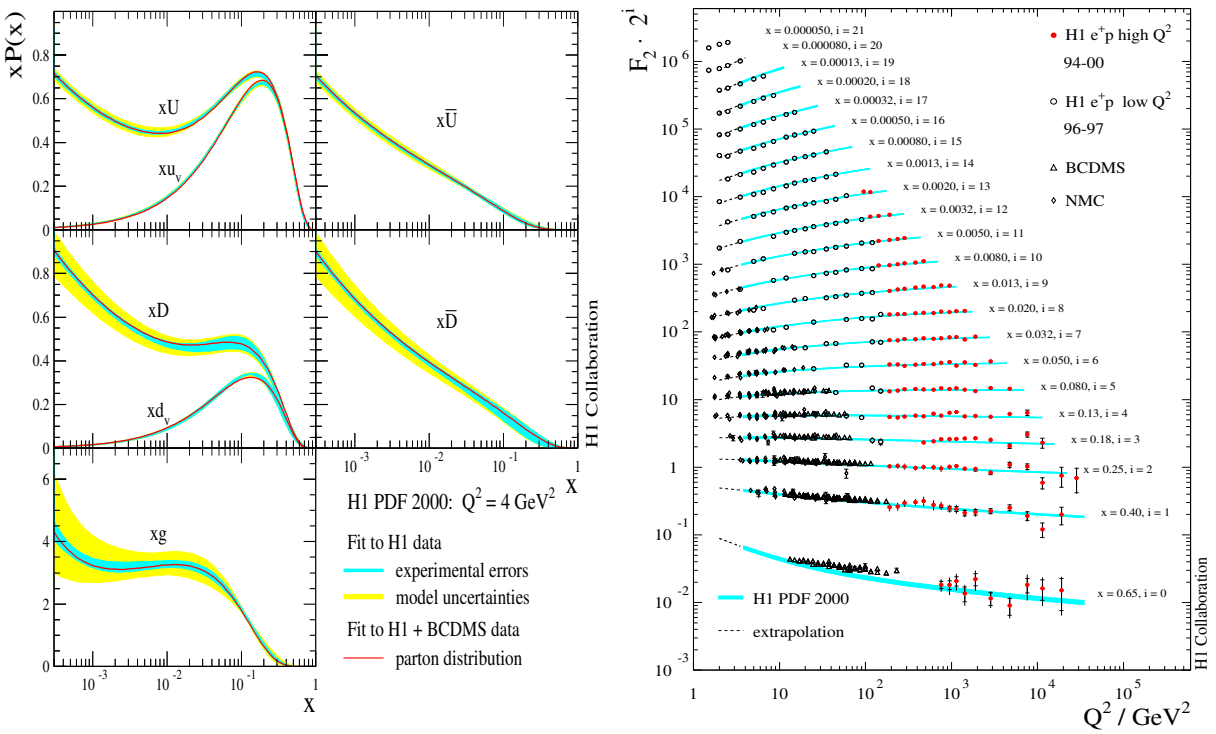

Figure 1: Left: PDFs $xU = x(u + c)$, $xD = x(d + s)$, $x\bar{U} = x(\bar{u} + \bar{c})$, $x\bar{D} = x(\bar{d} + \bar{s})$, and xg as determined from H1 fits at the starting scale $Q_0^2 = 4$ GeV^2. Right: F_2 from H1 and fixed target experiments compared to the H1 PDF 2000 fit.

The present accuracy of measurements, which is 2-3 % in the most of the kinematic region, allows to perform a NLO QCD fit to the H1 data alone. The H1 PDF 2000 fit [6] to the NC and CC cross sections determines the momentum distributions of gluons x$g(x)$ and of four quark combinations $xU = x(u + c)$, $xD = x(d + s)$, $x\bar{U} = x(\bar{u} + \bar{c})$, $x\bar{D} = x(\bar{d} + \bar{s})$, from which the valence densities $u_v = U - \bar{U}$ and $d_v = D - \bar{D}$ are derived. The resulting PDFs at the starting scale of $Q_0^2 = 4$ GeV^2 are displayed in fig. 1 (right).

The comparison of the H1 fit with the most recent H1 results on F_2 together with data from fixed target experiments is shown in fig. 1 (left). The data are well described by the DGLAP evolution over four orders of magnitude in Q^2 and in the range of x from $\sim 10^{-4}$ to 0.65. At small value of x the behavior of F_2 is dominated by the gluon emission.

In the high Q^2 region the generalized structure function $x\tilde{F}_3$ can be determined from the difference of the cross sections 1 of $e^{\pm}p$ scattering, $x\tilde{F}_3 = [\frac{d^2\sigma^-_{NC}}{dxdQ^2} - \frac{d^2\sigma^+_{NC}}{dxdQ^2}]/(2Y_-)$. Fig. 2 (left) shows x-dependence of $x\tilde{F}_3$ which is in good agreement with the QCD prediction within rather large statistical errors. The reduced cross sections for charge current interactions of positrons are depicted in fig. 3 (right) up to the highest reachable Q^2 values. The results are consistent with the H1 PDF 2000 fit. The contribution of down quarks is increasing with x.

A direct extraction of F_L requires measurements of $d^2\sigma/dxdQ^2$ at fixed x and Q^2 for different values of y, i.e. at sufficiently different center-of-mass energies. Since this option is up to now not available at HERA an indirect determination of F_L has been

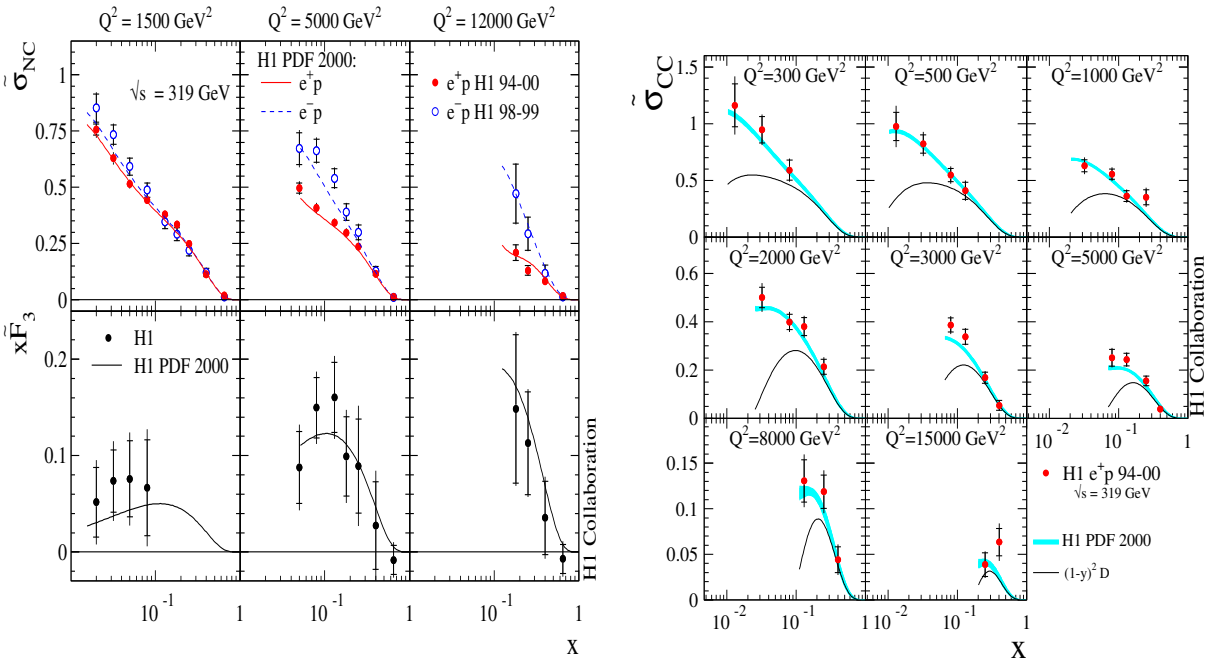

Figure 2: Left: The reduced cross sections $\tilde{\sigma}_{NC} = \frac{xQ^4}{2\pi\alpha}\frac{d^2\sigma^-_{NC}}{dxdQ^2}$ and $x\tilde{F}_3$. Lines represent the H1 PDF 2000 fit. Right: The reduced charge current cross section defined in eq. 3 as a function of x for several Q^2 bins. Thick bands correspond to the H1 PDF 2000 fit, solid lines to the down quark contributions, $D = x(d + s)$.

developed by the H1 collaboration [7, 8]. For Q^2 up to 1000 GeV^2 the contributions from Z^0 exchange can be neglected. In this range a determination of F_L is possible but at high values of y only, due to the term y^2 in the cross section 1. Several methods have been used which are based on the different behavior of the measured reduced cross section $\sigma_r = \frac{d^2\sigma^{\mp}_{NC}}{dxdQ^2}\frac{xQ^4}{2\pi\alpha^2 Y_+} = F_2 - \frac{y^2}{Y_+}F_L$ and F_2 extrapolated to high y using low y data (Fig. 3 (left)). The cross section measurements at high y where the scattered electron energies decreases to 3 GeV were facilitated with the help of the backward silicon tracker and the calorimeter SpaCal. Fig. 3 (right) shows the Q^2 dependence of F_L at fixed center-of-mass energy of the γp system, $W \approx \sqrt{y \cdot s - Q^2} = 276$ GeV, which corresponds to $y \approx 0.75$. The data points are in good agreement with most of theoretical models. The MRST 2001 NLO prediction [9] describes data in higher Q^2 region only.

3 Heavy Flavor Production

The investigation of the production of c and b quarks is considered as a convenient way of testing of QCD. At HERA the heavy flavor quarks are predominantly produced by the photon gluon fusion process (PGF) $\gamma g \to q\bar{q}\,(q = c, b)$. Two different Q^2 ranges are accessible at HERA: the photoproduction ($Q^2 \approx 0$) where the resolved photon interactions play important role and DIS ($Q^2 > 2$ GeV^2).

The theoretical calculations of open heavy production have been performed in three

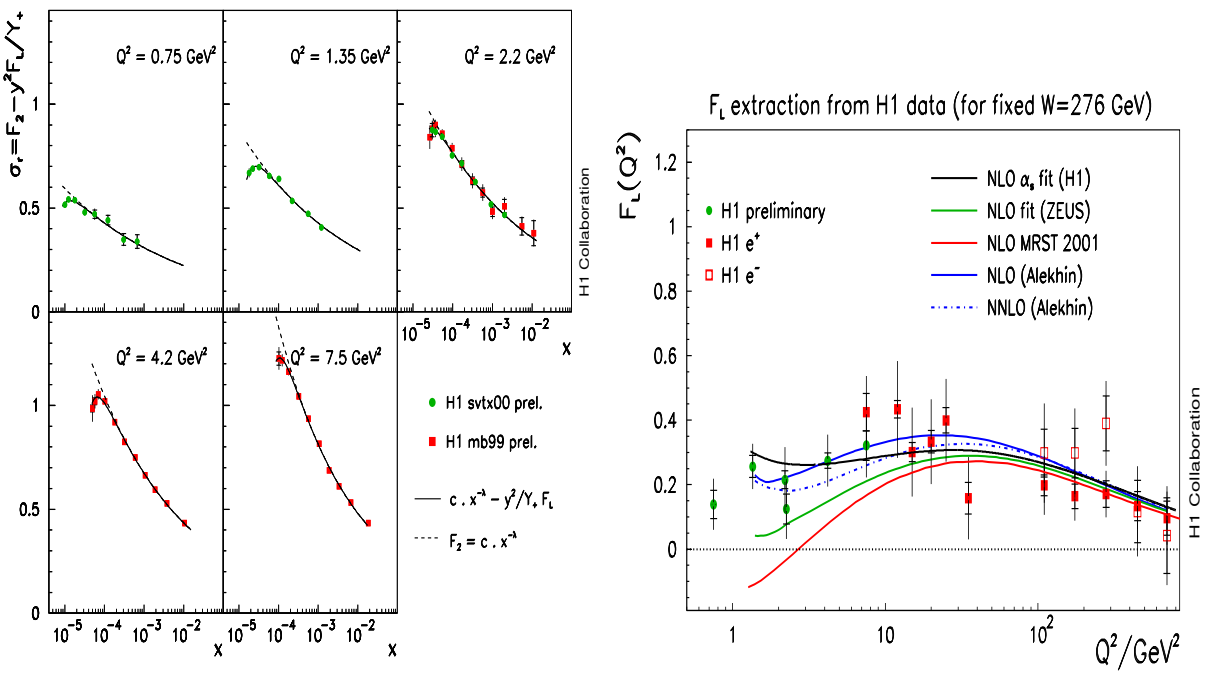

Figure 3: Left: The measured reduced cross section. The solid lines correspond to the fit, from which F_L is extracted. The dashed line represents the F_2 contribution to σ_r. Right: The Q^2 dependence of F_L at fixed W, summarizing the F_L values from the H1 experiment.

different NLO schemes. In the range of heavy quark transverse momentum $p_T \leq m_{c,b}$ the fixed order massive scheme, which is applied in the programs HVQDIS [10] and FMNR [11] for DIS and γp interactions respectively, gives reliable results. In this scheme heavy quarks are created by the PGF. The massless approach [12] valid for $p_T >> m_{c,b}$ treats the heavy quarks as sea quarks in the proton or in the resolved photon. In the third scheme (FONLL) both methods are combined [13]. The QCD calculations are complemented by the quark fragmentation functions, which enable to estimated inclusive heavy meson cross sections.

The experimental data are compared as well with LO Monte Carlo models where the higher orders are approximated by parton showers. Most of them like AROMA, PYTHIA, HERWIG, RAPGAP apply DGLAP evolution of parton densities. The CCFM evolution equations [14] are included in the Monte Carlo generator CASCADE [15], which uses unintegrated gluon densities extracted from H1 F_2 data.

3.1 Production of D Mesons

From the measurements of the visible inclusive D meson cross sections the relative fragmentation factors $f(c \to D)$ can be determined. They are given by the ratios of the production cross section of a specific charm meson to the sum of all charmed hadron cross sections. The comparison of values of $f(c \to D)$ with those from e^+e^- interactions confirms the validity of the hypothesis of the universality of the charm fragmentation.

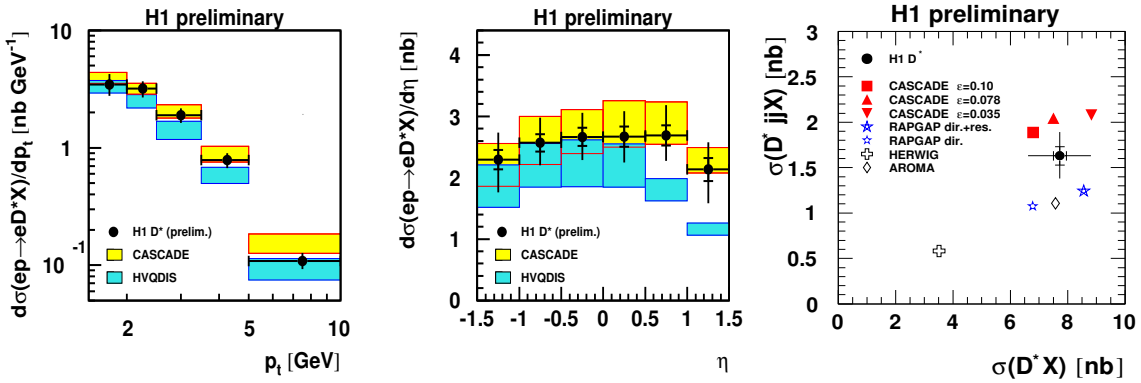

Figure 4: Left and center: Single inclusive cross section $\sigma(ep \to eD^{*\pm}X)$ versus p_t and η of the D^* meson. Lower shaded band corresponds to the HVQDIS calculations and upper shaded area represents a CASCADE simulation. Right: Measured D^* inclusive and dijet cross sections compared with predictions of various Monte Carlo generators.

For example the H1 fragmentation ratios for D^* were estimated to be [16]

$$f(c \to D^*)_{DIS} = 0.263 \pm 0.019^{+0.056\,+0.031}_{-0.049\,-0.022} \qquad f(c \to D^*)_{e^+e^-} = 0.235 \pm 0.010$$

where the errors of f_{DIS} correspond to the statistical, systematic and theoretical uncertainties.

The comparison of experimental data with theoretical predictions is illustrated in fig. 4 where the differential inclusive D^* cross sections in DIS are depicted. The agreement either with the HVQDIS calculations or the CASCADE simulation is good except at the high pseudorapidy η values. To study the D^* production mechanism in more detail the events with two jets in addition to D^* were selected [17]. The correlation between inclusive and dijet cross sections compared with several MC generator predictions is shown in fig. 4 (right). The CASCADE results with three modifications of Peterson fragmentation function are larger than the experimental value, whereas other models give too low values. Within the selected theoretical parameters explored in this analysis, none of the model is able to describe simultaneously both cross sections.

A similar comparison of inclusive D^* cross sections in γp interactions with theoretical estimates is shown in fig. 5, where $d\sigma/d\eta(D^*)$ is plotted [18]. The NLO QCD calculation in three flavor massive scheme is systematically below the data points. The four flavor massless prediction exhibits better agreement, but is very sensitive to the renormalisation and factorisation scales, which were chosen as $2\mu_r = \mu_f = 2\sqrt{m_c^2 + p_{T,c}^2}$. The limits plotted in fig. 5 (left) correspond to the changes of $\mu_{r,f}$ by the factors of 0.5 and 2. None of the two MC generators, PYTHIA and CASCADE, describes the cross section dependence on $\eta(D^*)$.

3.2 Beauty Production

Beauty production at HERA is suppressed by two orders of magnitudes with respect to the $c\bar{c}$ cross section. On the other hand the investigation of final states containing b quark

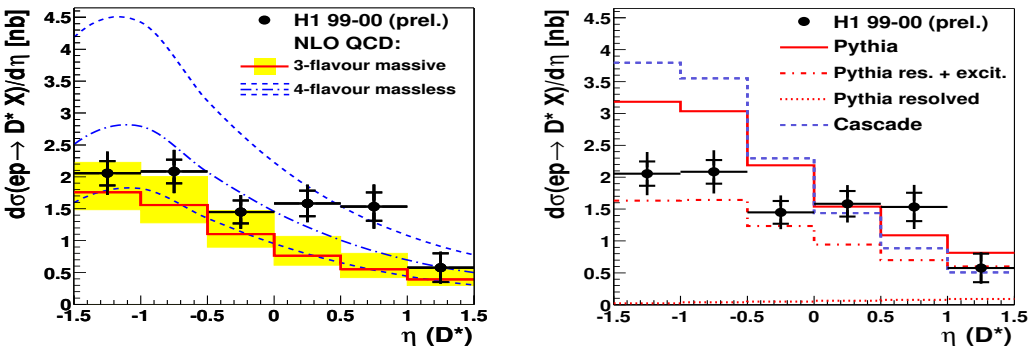

Figure 5: Differential cross section $d\sigma(ep \to eD^{*\pm}X)/d\eta$ compared with NLO QCD calculations (left) and with two Monte Carlo predictions (right).

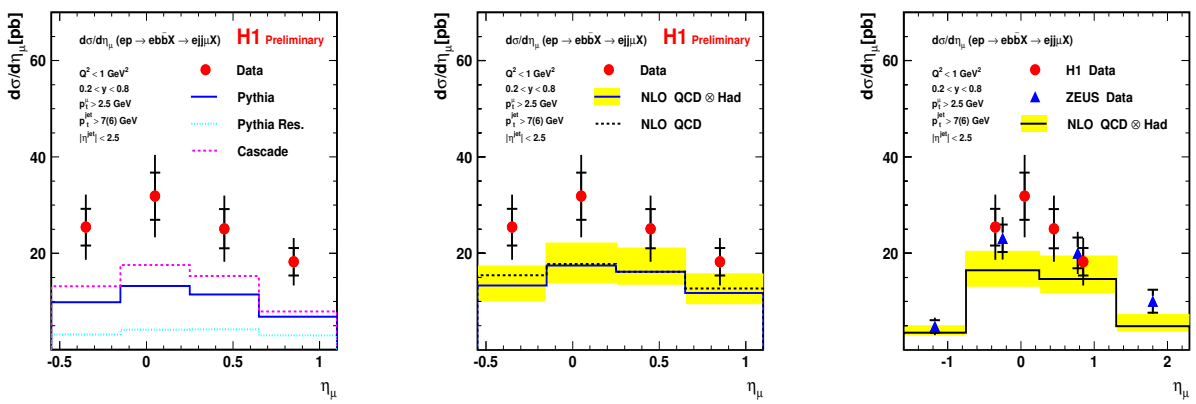

Figure 6: Differential cross section $\sigma_{vis}(ep \to eb\bar{b} \to ejj\mu X)$ measured in the photoproduction. Left: The comparison with the PYTHIA and CASCADE simulations. Center: The comparison with NLO QCD calculations. Right: The comparison with ZEUS data.

is expected to be very important since theoretical predictions should be more reliable due to the large mass m_b. Beauty events were tagged by the b decays into muons of high transverse momentum, p_T^{rel}, relative to the jet axis, which approximates the momentum direction of a B hadron. In addition, H1 takes advantage of relatively long decay length of beauty hadrons by measuring the impact parameter δ of the decay muon in the precise central silicon vertex detector.

The previous measurements of the beauty inclusive cross sections showed a large excess over NLO QCD calculations, especially in γp interactions [19]. The higher event statistics now allows to determine the dijet-muon production cross section. In the recent H1 analysis [20] events with 2 jets and a muon were selected in the kinematic range of $Q^2 < 1$ GeV^2, $0.2 < y < 0.8$, $p_T^\mu > 2.5$ GeV, $-0.55 < \eta^\mu < 1.1$, $p_T^{jet_{1(2)}} > 7(6)$ GeV and $|\,\eta^{jet}\,| < 2.5$. The cross section is measured to be

$$\sigma_{vis}(ep \to eb\bar{b} \to ejj\mu X) = 42.5 \pm 3.4(stat) \pm 8.9(syst)\,\text{pb}$$

The NLO QCD predictions of modified fixed order massive program FMNR [21] gives $(24.1^{+7.2}_{-5.1})$ pb, which is within 1.5 limit of the combined errors of both values. This difference between the measured and calculated cross sections is smaller than the one previously published.

The cross section $d\sigma/d\eta_\mu$ is compared with NLO calculations and PYTHIA and CASCADE simulations in fig. 6 (right). The theoretical predictions fails to describe data in the whole explored kinematic region. H1 results are consistent with the ZEUS analysis which includes data from the larger kinematic region, as it is demonstrated in fig. 6 (right).

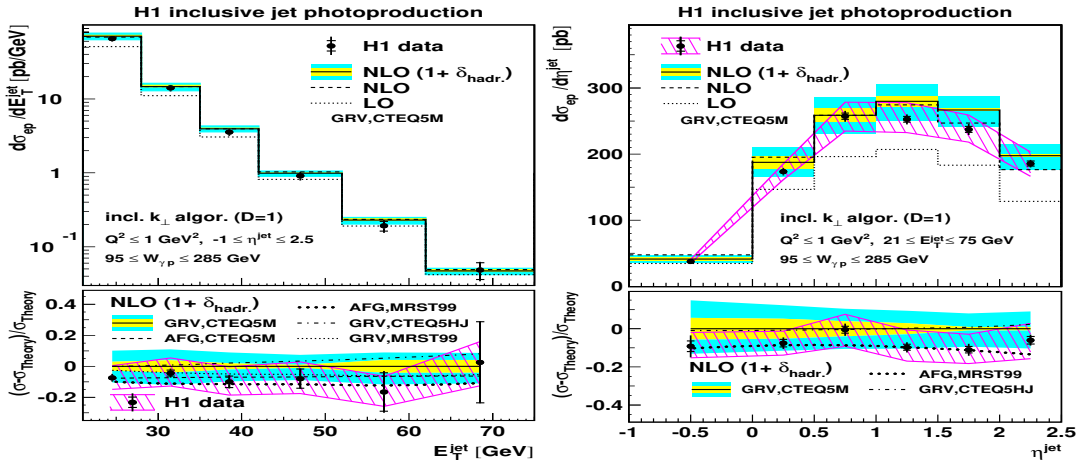

Figure 7: Left top: Inclusive jet cross section $d\sigma/dE_T^{jet}$. Right top: Inclusive jet cross section $d\sigma/d\eta^{jet}$. Data are compared with LO and DGLAP NLO QCD calculations using GRV photon PDFs and CTEQ5M proton PDFs. Bottom: The relative difference between data and calculations (for details see text). The hatched bands correspond to the uncertainty associated with the LAr energy scale.

4 Hadronic Final States

Jet measurements at HERA offer a means of testing of the validity of perturbative QCD predictions. A detection of jets at high transverse energy E_T^{jet} may be used to investigate the dynamics of the exchanged parton cascade. On the other hand, single particle or resonance spectra provide an opportunity to study quark hadronisation, which cannot be treated within the QCD theory.

Recent H1 results concern the inclusive jet production in γp interactions [22], the study of dijet and three jet event shapes [23] in DIS, the dijet [24] and forward jet [25] production in DIS. In addition, differential cross sections of prompt photons [26], π^0 [27], and resonances η, ρ, f_0 and f_2 [28] have been determined. In this article we will focus on jet results.

The cross sections of inclusive jet production as a function of E_T^{jet} and the rapidity η^{jet} are shown in Fig. 7 (top). The NLO QCD calculations of the basic partonic cross sections [29] supplemented by the hadronic corrections are in good agreement with the data. The dependence of the theoretical predictions on the photon PDFs (GRV or AFG) and

proton PDFs (CTEQ5M, CTEQ5HJ, MRST99) is illustrated in Fig. 7 (bottom). The contributions of two uncertainty sources to the theoretical error, hadronic correction and the renormalisation and factorisation scales, are shown by the shaded bands.

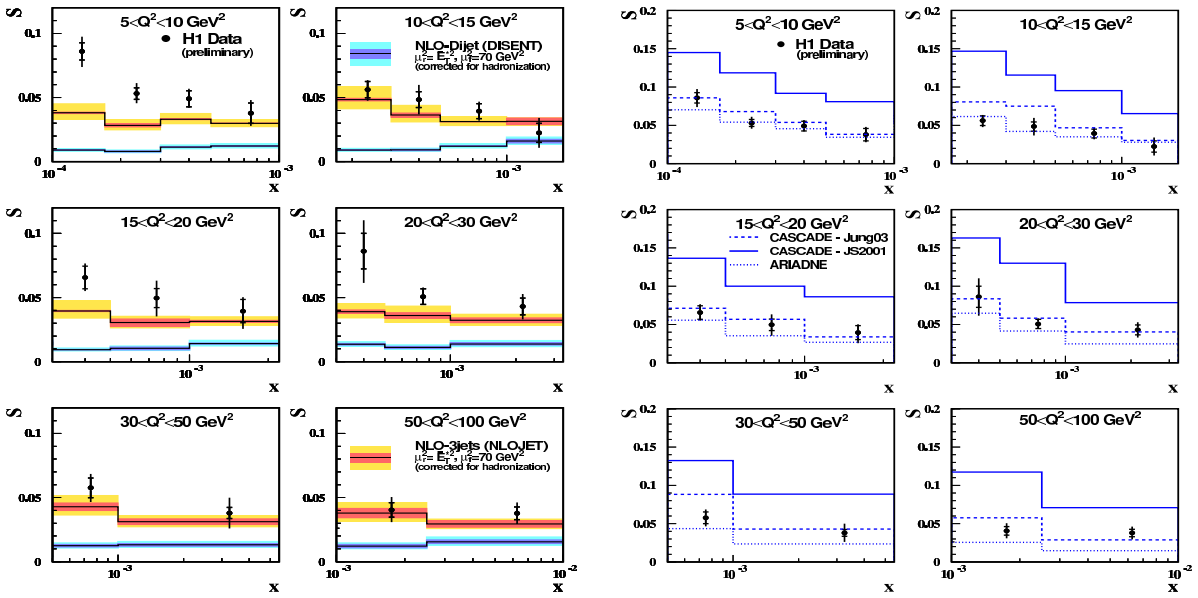

Figure 8: Ration S of events with small azimuthal separation ($\Delta\Phi < 120^o$) of the two most energetic jets with respect to the total number of inclusive dijet events. Data are compared with NLO dijet and 3-jet calculations and with predictions from ARIADNE and CASCADE.

More detailed information about the dynamics of the parton cascade can be obtained by investigating dijet events in DIS at very low x. In this kinematic range a deviation from DGLAP scheme is most likely to be observed, since an alternative approach to the parton shower evolution like BFKL or CCFM is more appropriate. In the H1 accessible region of x between 10^{-4} and 10^{-2} the triple differential cross section $d^3\sigma/(dxdQ^2dE^*_{Tmax})$ was found to be in good agreement [24] with the DGLAP NLO QCD calculations, which were performed using the program DISENT [29]. The further insight into small x-dynamics may be gained by studying behavior of events with small azimuthal separation $\Delta\Phi^*$ between the two jets in the hadronic-center-of mass system. The basic parton interactions in DGLAP formalism proceed via partons of small transverse momenta k_t. In the leading order the back-to-back two jet configuration can be expected with $\Delta\Phi^* \approx 180^o$. In the BFKL or CCFM models a significative proportion of partons entering hard processes is created with large k_t, which leads to the smaller $\Delta\Phi^*$ separation. The ration S of events with $\Delta\Phi^* < 120^o$ over all 2 jet events is shown in fig. 8 as a function of x and Q^2. The DISENT prediction gives too low values of S. The NLO 3-jet calculation NLOJET [30] describes data better, but a difference is visible at low x and low Q^2. A good agreement is also achieved by the program CASCADE with the suitable unintegrated gluon densities (Jung 2003) and by the program ARIADNE, which generates non-k_t ordered parton cascades using the color dipole model.

The difference between various dynamical approaches to the parton shower cascades

is also expected in the production of forward jets which are emitted in the angular range close to the proton beam. In the DGLAP formalism the corresponding cross section is small if $p^2_{T,jet} \approx Q^2$. In the CCFM model the forward jet rate in DIS at large Q^2 and at small x rises with x. The dependence of the corresponding cross section on x is depicted in fig. 9. The data are compared with the ARIADNE and CASCADE simulations and

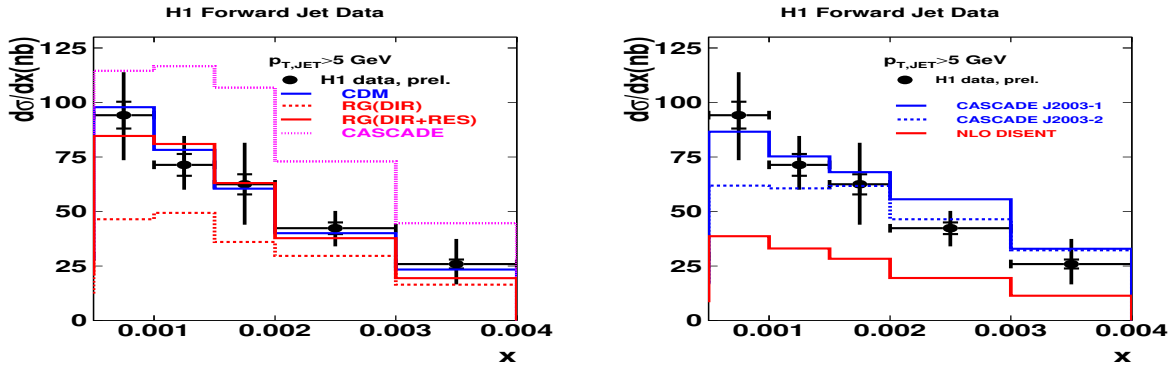

Figure 9: The cross section for forward jet production as a function of x. Left: Data are compared to the predictions from the ARIADNE (CDM), RAPGAP (RG) and CASCADE Monte Carlos. Right: The same data are compared with the DISENT calculations and the CASCADE simulations with two different unintegrated gluon densities.

to the RAPGAP Monte Carlo generator, which is based on the DGLAP scheme (fig. 9 (left)), and to the DISENT calculation and to the predictions of CASCADE with two versions of unintegrated gluon densities (fig. 9 (right)). The NLO DISENT results and RAPGAP with direct photons do not describe data. Other Monte Carlo models give good agreement with the data within experimental errors. It seems, that in the low x range the H1 data favor non-DGLAP evolution formalism. On the other hand RAPGAP with resolved and direct photons agrees also well with the experimental results.

5 Diffraction

Diffractive processes in $\gamma^* p \to XY$ interactions at HERA lead to observation of the large rapidity gap between hadronic systems X and Y, which originates from the dissociations of the proton and the virtual photon. At high energies this dissociation is dominated by the pomeron[3] exchange mechanism. The previous HERA measurements have indicated that the parameters of the pomeron trajectory in the soft scattering differ from those in the hard scattering, i.e. the intercept of the pomeron trajectory, α_0, changes from ~ 1.08 to ~ 1.20.

To describe kinematics of diffractive DIS the new additional variables $x_{I\!P}$ and β are introduced, which define the longitudinal momentum fraction of the proton carried by the pomeron $I\!P$ and the longitudinal momentum fraction of the pomeron carried by the struck quark. Here, β has an analogous interpretation in $\gamma I\!P$ collisions as x-Bjorken in the

[3]Here we use the notation pomeron for any colorless exchange.

γp interactions. Moreover, the diffractive processes depend on the momentum transfer t between the initial proton and the proton dissociation system.

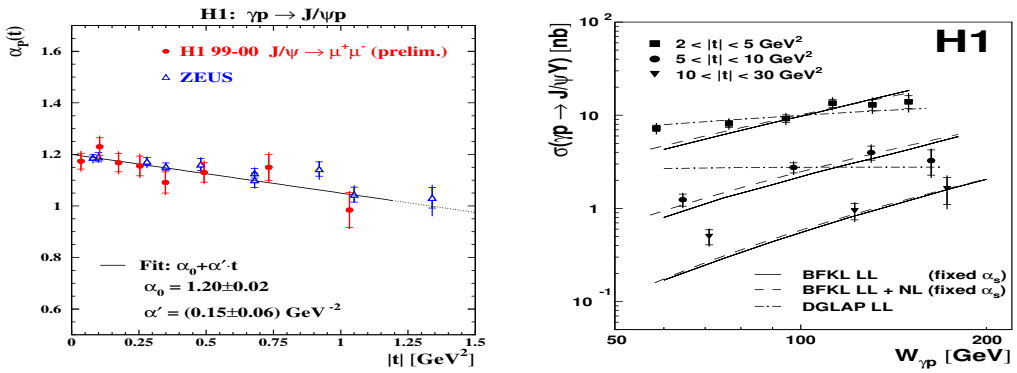

Figure 10: Left: The effective pomeron trajectory as a function of $\mid t \mid$. Right: The diffractive J/ψ cross section as a function of $W_{\gamma p}$ in three bins of $|t|$.

The QCD calculations are based on the factorisation theorem, which implies that the diffractive cross sections in $\gamma^* p$ processes can be expressed in terms of convolutions of universal partonic cross sections with proton diffractive partonic distributions $f_i^D(t, x_{IP}, Q^2, \beta)$. An additional factorisation assumption is usually made about the dependence of f_i^D on the kinematic variables, i.e. $f_i^D = f_{IP/p}(x_{IP}, t) f_{i/IP}(\beta, Q^2)$, where the first term is the pomeron flux and the second one corresponds to parton densities of the diffractive processes.

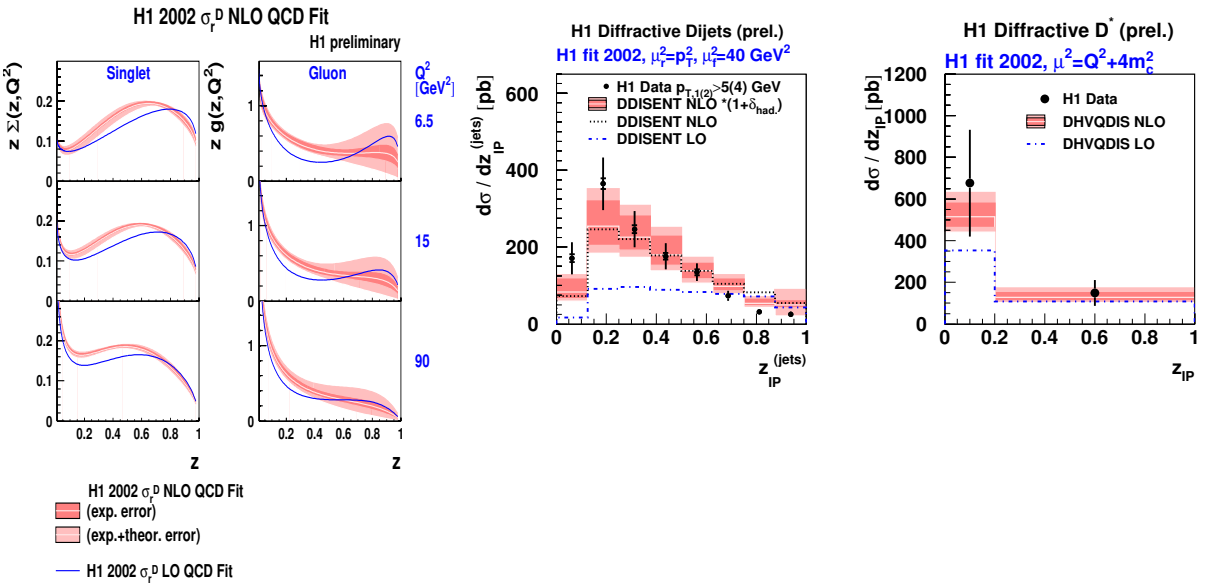

Figure 11: Left: Diffractive singlet quark ($6 * u$ with $u = d = s = \bar{u} = \bar{d} = \bar{s}$) and gluon distributions. Diffractive DIS dijet (center) and D^* meson (right) cross sections compared with the DISENT and HVQDIS calculations.

Some of the recent H1 results come from the investigation of elastic and diffractive photoproduction of J/ψ mesons. From fits [31] of the differential cross sections $d\sigma(\gamma p \to J/\psi p)/dW_{\gamma p}$ in several bins of $|\,t\,|$ the dependence of the pomeron trajectory (fig. 10), $\alpha_{IP/p}$, on the momentum transfer was extracted, $\alpha_{IP/p} = (1.20 \pm 0.02) + (0.15 \pm 0.06) \cdot t$. The higher intercept of $\alpha_{IP/p}$ and the effect of shrinkage is observed. The differential cross sections [32] of the interaction $\gamma p \to J/\psi Y$ are plotted in fig. 10 (right) as a function of $W_{\gamma p}$ in three bins of $|t|$. At large momentum transfer $|t| > 5$ GeV^2 they are well described by QCD calculations using the BFKL model.

From the measurements of the inclusive diffractive cross section [33] integrated over t the single diffractive quark and gluon densities, shown in fig. 11, have been determined [34]. Here, the variable z corresponds to the momentum fraction carried by an individual parton and the lines represent results of LO fits and bands NLO fits. The diffractive exchange is dominated by gluons, which carry high fractional momenta, e.g. 75 ± 15 % at $Q^2 = 10$ GeV^2. These parton densities are used to describe semi-inclusive cross sections for dijet and open charm production in DIS [35]. In fig. 11 the dijet diffractive and D^* cross sections are displayed as a function of the fractional momentum z_{IP} of the pomeron exchange entering the hard scattering. The NLO calculations of DISENT and HVQDIS, corrected for hadronisation effects, provide a reasonable description of the measured cross sections within the experimental errors and therefore they confirm the hypothesis of the factorisation in diffractive DIS.

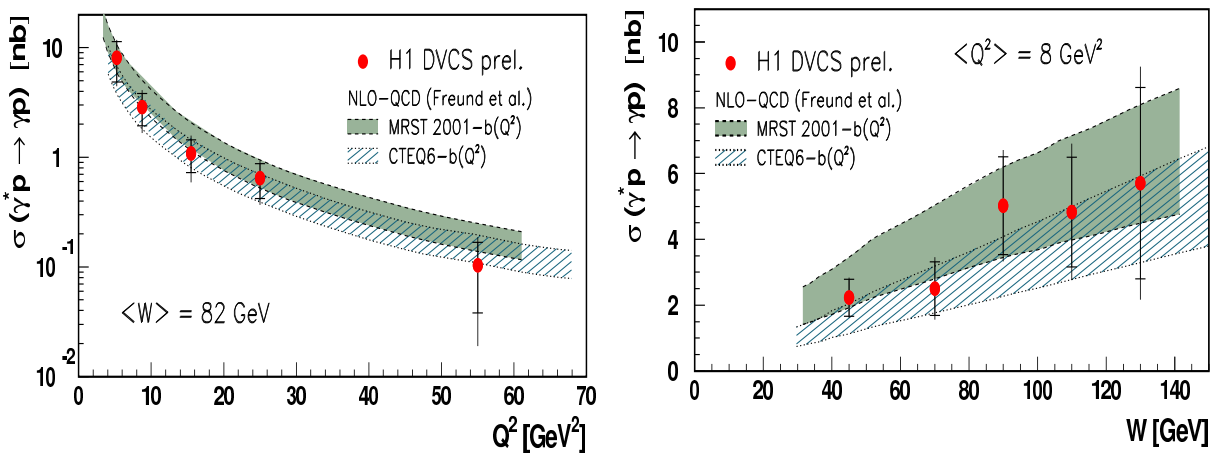

Figure 12: The $\gamma^* p \to \gamma p$ cross sections compared with NLO QCD predictions [37] using two different GPD parametrisation and t dependence as e^{bt}, with $b = b_0(1 - 0.15 \cdot log(Q^2/2))$ GeV^{-2}. The bands correspond to b_0 values between 5 and 9 GeV^{-2}.

The deeply virtual Compton scattering (DVCS) process $\gamma^* p \to \gamma p$ is suitable for testing of BFKL evolution. The cross section [36] of this interaction is shown in fig. 12 as a function of W and Q^2. The data are compared with the theoretical prediction [37] which uses generalized parton densities (GPD) modified by an exponential dependence on t. The agreement is satisfactory within the experimental and theoretical uncertainties.

6 Search for new physics

The H1 experiment has searched for signals beyond the Standard Model (SM) by investigating hard processes in ep-scattering. At large Q^2 a deviation of the observed cross

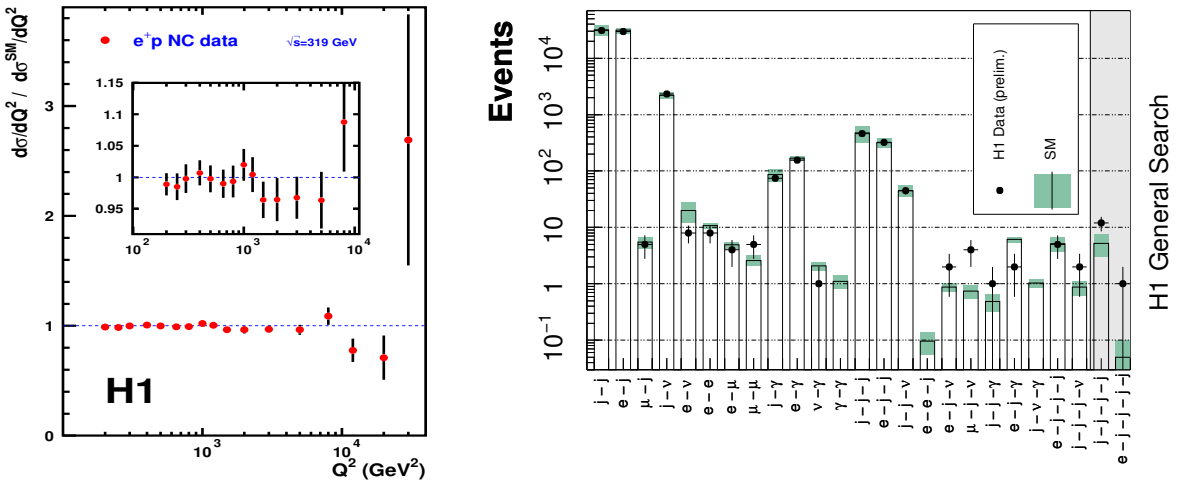

Figure 13: Left: Comparison of measured cross section with Standard Model (SM) predictions. Right: The measured and expected event yields for all considered event classes.

sections from the SM predictions can be caused for example by the exchange of a new heavy boson. Indirect signature of this effect can be found by analyzing data in the framework of contact interactions.

Fig. 13 (left) shows good agreement between measured e^+p differential cross section and SM calculations in the whole available Q^2 range. This result sets the lower limits on the compositness scale parameter Λ, which are between 1.6 TeV and 5.5 TeV depending on the chiral structure of the Lagrangian of four-fermion contact interactions [38].

Other tests of various models have been performed and upper limits on the cross sections of new processes have been derived. For example possible squark production in R parity violating supersymmetry have been studied recently [39]. All these models lead to different final state event topologies. The H1 has made a general search for deviations of event yields of twenty different final state configurations from SM predictions not relying on specific models [40]. A topology class is assigned to events in which an isolated final state object with $p_T > 20$ GeV, like jet (j), electron, muon, γ or missing momentum was identified. The significance of a deviation is based on two estimators, total transverse momentum of objects and total effective mass of all objects, which are sensitive to new physics signals. The result for different final state configurations is displayed in fig. 13 (right). The shaded areas represent the total systematic errors of the calculations. A discrepancy between data and SM expectation is observed in the $\mu - j - \nu$ topological class, where 4 events were observed and 0.7 ± 0.2 are expected. The effective mass M_{all} for this object configuration is depicted in fig. 14 (left).

The H1 has reported the event excess in a more detailed analysis [41] of events with isolated electrons and muons and missing momentum. Here, more specific criteria for

event selection were applied. The distribution of the transverse momentum p_T^X of the hadronic system is shown in fig. 14 (right) for the events with a lepton of the transverse momentum greater than 10 GeV .The dominant SM process at high p_T^X is the interaction $ep \to e(\nu) + W^{\pm} + X$. For $p_T^X > 25$ GeV, 10 events were found compared to the expected

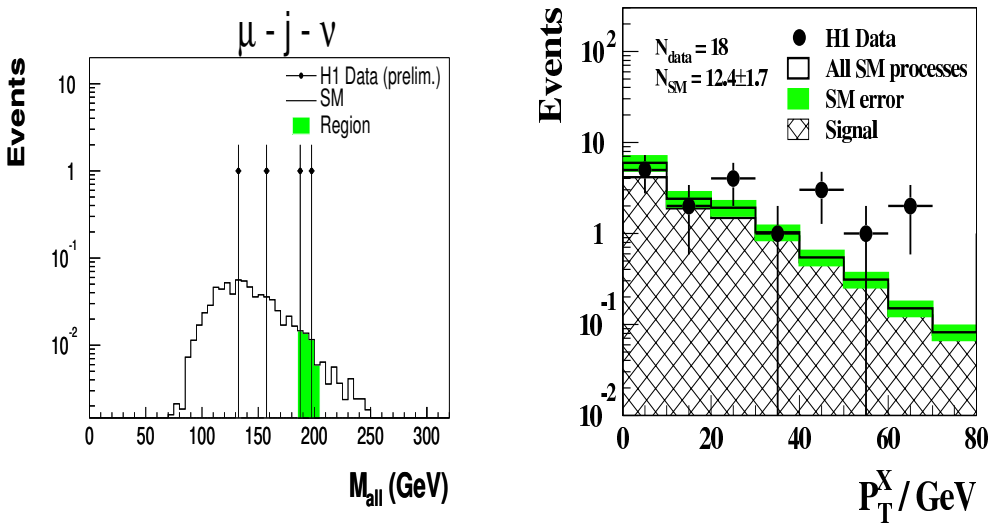

Figure 14: Left: The distribution of total effective mass M_{all} for the event class $\mu - j - \nu$. The shaded region shows the region of the greatest deviation from the SM expectation. Right: The distribution of transverse momentum of the hadronic system for the events with an isolated muon or electron and missing momentum. The hatched histogram correspond to the SM expectation. The total error of the SM prediction is given by the shaded band.

number of 2.92 ± 0.49.

Since the above mentioned event topology is similar to the object configuration coming from a top, decaying semileptonically, $t \to bW \to bl\nu$, a possible explanation of the the event excess could be a non-standard top production via flavor changing neutral currents. From the observed events exclusion limits on the corresponding coupling constants have been determined [42].

Another deviation from SM prediction has been found in the multi-electron events [43]. An excess of three di-electron and three tri-electron events with di-electron invariant masses greater than 100 GeV above SM expectation was observed. The corresponding SM predictions are 0.30 ± 0.04 and 0.23 ± 0.04.

7 Summary

Some of the most recent H1 results obtained in the analysis of the data from the first phase of HERA running are presented.

The proton structure functions from the range $1 < Q^2 < 10^4$ GeV^2 were extracted from the measurements of the neutral and charged current cross sections. The QCD fits of the NC cross section provide the quark and gluon densities in the region $10^{-4} < x < 0.65$.

New measurements of the open charm production show, that the QCD calculations cannot describe all aspects of the data behavior. The beauty differential cross sections in the experimentally visible region are in better agreement with NLO calculations than the previous published total cross section.

Many features of inclusive jet or two jet production can be explained by the QCD including the DGLAP evolution equations. The investigation of events with two jets or a forward jet in the small x region seems to indicate that the standard DGLAP evolution is insufficient to describe the data and CCFM evolution may be more appropriate for the parton showering in this kinematic range.

The analysis of diffractive events supports the hypothesis of the Regge factorisation with a value for the pomeron intercept which is bigger than for the soft pomeron. The J/ψ diffractive cross sections at large momentum transfer are reasonably described by the BFKL model. Similarly, the behavior of the cross section of the deeply virtual Compton scattering $\gamma^* p \to \gamma p$ can be understood within a model which includes generalized parton densities. The new QCD fits of diffractive DIS cross sections result in the proton diffractive parton densities which give consistent description of hadronic final states in diffractive DIS.

The general agreement between data and Standard Model predictions in hard processes in ep-interactions is good. Two deviations have been observed in the events with an isolated lepton of high p_t and missing transverse momentum and in multi-electron events.

Acknowledgments

This work was supported by the Ministry of Education of the Czech Republic under the project INGO-LA116/2000. I would like to thank M. Klein and V. Chekelian for help with the preparation of this presentation and for reading this manuscript.

References

[1] I. Abt et al., [H1 Collaboration], Nucl. Instrum. and Meth. A386 (1997) 310

[2] I. Abt et al., [H1 Collaboration], Nucl. Instrum. and Meth. A386 (1997) 348

[3] D. Pitzl et al., Nucl. Instrum. and Meth. A454 (2000) 334

[4] W. Eick et al., Nucl. Instrum. and Meth. A386 (1997) 81

[5] R. D. Appuhn et al., Nucl. Instrum. and Meth. A386 (1997) 397

[6] C. Adloff et al., [H1 Collaboration], Eur. Phys. J. C30 (2003) 1

[7] C. Adloff et al., [H1 Collaboration], Eur. Phys. J. C19 (2001) 33

[8] H1 Collaboration, contributed paper 83 to EPS 2003, Aachen

[9] A. D. Martin, R. G. Roberts, W. J. Stirling and R. S. Thorne, Eur. Phys. J. C23 (2002) 73

[10] B. W. Harris and J. Smith, Phys. Rev. D57 (1998) 2806

[11] M. L. Mangano, P.Nason and G. Ridolfi, Nucl. Phys. B373 (1992) 295; S. Frixione et al., Nucl. Phys. B412 (1994) 225

[12] B. A. Kniel et al., Z. Phys. C76 (1997) 689; J.Binnewies et al., Phys. Rev D58 (1998) 014014; M. Cacciari and M.Greco, Phys. Rev. D55 (1997) 7134
[13] M. Cacciari, S. Frixione and P. Nasen, hep-p4/0102134
[14] M. Ciafaloni, Nucl. Phys. B296 (1988) 49; S. Catani, F. Fioriani and M. Marchesini, Phys. Lett. B234 (1990) 339
[15] H. Jung and G. P. Salam, Eur. Phys. J. C19 (2001) 351
[16] H1 Collaboration, contributed paper 96 to EPS 2003, Aachen
[17] H1 Collaboration, contributed paper 98 to EPS 2003, Aachen
[18] H1 Collaboration, contributed paper 97 to EPS 2003, Aachen
[19] C. Adloff et al., [H1 Collaboration], Phys. Lett. B467 (1999) 156
[20] H1 Collaboration, contributed paper 117 to EPS 2003, Aachen
[21] S. Frixione et. al., Phys. Lett. B348 (1995) 633
[22] C. Adloff et al., [H1 Collaboration], DESY preprint 02-225, 2002
[23] H1 Collaboration, contributed paper 111 to EPS 2003, Aachen
[24] A. Aktas et al., [H1 Collaboration], DESY preprint 03-160, 2003 two jet at low x
[25] H1 Collaboration, contributed paper 109 to EPS 2003, Aachen
[26] H1 Collaboration, contributed paper 93 to EPS 2003, Aachen
[27] H1 Collaboration, contributed paper 86 to EPS 2003, Aachen
[28] H1 Collaboration, contributed paper 107 to EPS 2003, Aachen
[29] C. Catani and M. H. Seymour, Nucl. Phys. B485 (1997) 29
[30] Z. Nagy and Z. Troscanyi, Phys. Rev. Lett. 87 (2001) 082001
[31] H1 Collaboration, contributed paper 109 to EPS 2003, Aachen
[32] A. Aktas et al., [H1 Collaboration], Phys. Lett. B568 (2003) 205
[33] H1 Collaboration, contributed paper 90 to EPS 2003, Aachen
[34] H1 Collaboration, contributed paper 89 to EPS 2003, Aachen
[35] H1 Collaboration, contributed paper 113 to EPS 2003, Aachen
[36] H1 Collaboration, contributed paper 115 to EPS 2003, Aachen
[37] A. Freund and M. McDermott, Eur. Phys. J. C23 (2002) 651
[38] C.Adloff et al., [H1 Collaboration], Phys. Lett. B568 (2003) 35
[39] H1 Collaboration, contributed paper 101 to EPS 2003, Aachen
[40] H1 Collaboration, contributed paper 118 to EPS 2003, Aachen
[41] V. Andreev et al., [H1 Collaboration], Phys. Lett. B561 (2003) 241
[42] A. Aktas et al., [H1 Collaboration], DESY preprint 03-132, 2003
[43] A. Aktas et al., [H1 Collaboration], Eur. Phys. J. C31 (2003) 17